ACS APPLIED MATERIALS & INTERFACES

Research Article

www.acsami.org

A Smart "Strider" Can Float on Both Water and Oils

Liming Qin, Jie Zhao, Shengbin Lei, and Qinmin Pan*

State Key Laboratory of Robotics and Systems, School of Chemical Engineering and Technology, Harbin Institute of Technology, Harbin 150001, People's Republic of China

Supporting Information

ABSTRACT: Aquatic devices that can work on both water and oils have great scientific and practical significance, but the challenge remains in developing novel materials with excellent repellence to both water and oils. Here, we report that an artificial "strider" can float on both water and oils by using supporting legs with ultraviolet (UV) switchable wettability. The legs were fabricated by immobilizing TiO_2 nanoparticles and *n*-dodecanethiol onto copper foams via a simple mussel-inspired process. At ambient conditions, the strider floated freely on a water surface, but it dived in water and then stood stably at the interface of water/$CHCl_3$ after UV illumination for 2 h. The reason for this unique behavior is that the legs changed their wettability from superhydrophobicity to underwater superoleophobicity after the illumination. It was revealed that the micro/nanohierarchical structures and photosensitivity of the immobilized TiO_2 nanoparticles accounted for the switchable wettability and large supporting force of the legs. The findings of this study offer an alternative strategy for fabricating smart aquatic devices that might be used for water environment protection, water resource surveillance, oil spill cleanup, and so on.

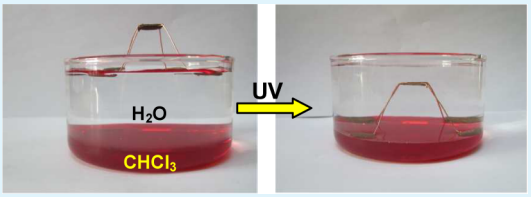

KEYWORDS: *smart aquatic device, UV switchable wettability, TiO_2 nanoparticles, mussel-inspired process, supporting force*

INTRODUCTION

Miniaturized aquatic devices that can move freely on a water surface are attracting considerable interest among scientists of multidisciplinary research.[1] Over the past few years, novel aquatic devices were developed by mimicking the unique walking capability of a water strider.[2] The key for these novel devices is to use artificial supporting legs that have excellent repellence to water.[3] Bioinspired interfacial functional materials, including superhydrophobic wires,[4−6] plates,[7] or foams,[8] had been employed as the supporting legs of the devices. These superhydrophobic legs produced large supporting forces at the water/air interface, which enabled artificial "water striders" to walk[9] and even jump[8] freely on a water surface. However, most of these aquatic devices could not work on an oily surface.

Recently, Liu et al. first proposed an "oil strider" that could freely float at the interface of water/oil by using superhydrophilic copper wires as supporting legs.[10] In spite of high affinity to water, these superhydrophilic wires displayed excellent oil-repellent properties in water, exhibiting interesting underwater superoleophobicity. As a result, the legs produced a large superoleophobic force to support the oil strider at the water/oil interface. The underwater superoleophobicity is believed to originate from highly hydrophilic components and micro/nanohierarchical structures of the legs.[10,11] Although a water strider and an oil strider have already been reported, a smart device capable of working on both water and oils is still lacking. Considering the complexity of water surface, especially for an oil-polluted aqueous environment, it is necessary and urgent to design a smart aquatic device that can move freely on both water and oils.

A main challenge for the above-mentioned smart device is the availability of interfacial materials exhibiting high repellence to both water and oils. Although using superamphiphobic surfaces might achieve the goal,[12,13] their fabrication usually involved complicated nanostructures and expensive fluorinated chemicals.[14−18] Moreover, most of superamphiphobic surfaces were only effective to a limited kind of oils, and they could not produce a large supporting force in aqueous environments. In contrast, a superhydrophilic surface is not only readily available but also exhibits excellent repellence to oils in aqueous conditions due to underwater superoleophobicity. More importantly, superhydrophilicity and superhydrophobicity is switchable under given stimuli,[19,20] such as ultraviolet (UV) irradiation,[21−26] thermal treatment,[27−29] changing pH,[30−32] or electric potential,[33] using an electric field,[34] ion exchange,[35] and so on.[36] Therefore, interfacial materials with switchable superhydrophobicity/superhydrophilicity might be a desirable choice for fabricating a smart miniaturized device working on both water and oils.

Inspired by this finding, herein, we report that an artificial strider can float on both water and oils via smartly changing wettability for the first time, while avoiding the use of complicated nanostructures and expensive fluorinated chemicals. The strider is supported by four artificial legs with switchable superhydrophobicity/superhydrophilicity that are fabricated through a facile mussel-inspired process.[37] After ultraviolet (UV) irradiation, the legs switch their wettability

Received: September 15, 2014
Accepted: November 17, 2014
Published: November 17, 2014

from superhydrophobicity to underwater superoleophobicity, which allows the strider to move from a water surface to the water/$CHCl_3$ interface (Scheme 1). The findings of this study offer an alternative strategy for designing smart aquatic devices that have potential applications in water environmental protection, water pollution surveillance, oil spill cleanup, and so forth.

Scheme 1. Illustration for the Fabrication of Copper Foams with UV Switchable Superhydrophobicity/Underwater Superoleophobicity

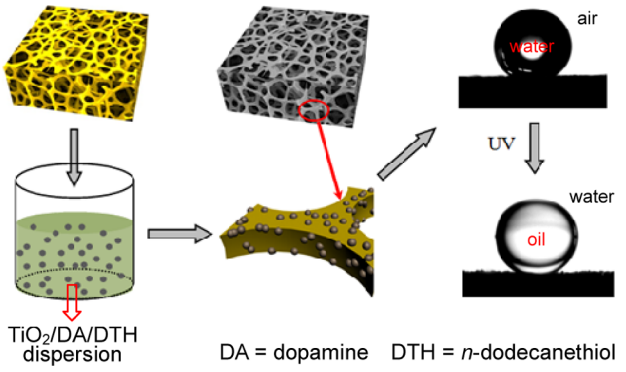

EXPERIMENTAL SECTION

Materials. Dopamine hydrochloric acid was supplied by BASF Corp. (Tianjin, China). Copper foams were provided by Wuzhou New Mater. Co., Ltd. (Guangxi, China). The copper foams were fabricated by electrodepositing copper on the surface of nickel foams. *n*-Dodecanethiol, tetrabutyl titanate, and isopropyl titanate were purchased from Aladdin Chemistry Co., Ltd. (Shanghai, China). Isopropyl alcohol and acetic acid were supplied by Fuyu Chemistry (Tianjin, China). Hydrofluoric acid was supplied by Kedi Chemical Reagent (Tianjin, China). Nitric acid was provided by Xilong Chemical Co., Ltd. (Shanghai, China).

Synthesis of TiO_2-30 Nanoparticles. Deionized water (3 mL), HNO_3 (6 mL) and tetrabutyl titanate (6 mL) were mixed with 60 mL of ethanol under stirring. Later 0.6 mL of hydrofluoric acid (HF, 40%) was added to the mixture. The resulting mixture was transferred to a Teflon-lined stainless steel autoclave and maintained at 180 °C for 36 h. After centrifugation, the powder was washed with ethanol three times and dried at 100 °C. The resulting powder was then sintered at 550 °C in air for 5 h to obtain TiO_2 nanoparticles with a diameter of ~30 nm (TiO_2-30 nanoparticles).

Synthesis of TiO_2-600 Nanoparticles. Acetic acid (3 mL) and isopropyl titanate (3 mL) were added to 30 mL of isopropyl ethanol under stirring. The resulting mixture was transferred to a Teflon-lined stainless steel autoclave and maintained at 160 °C for 24 h. After centrifugation, the powder was washed with ethanol three times and dried at 100 °C. The powder was sintered at 600 °C in air for 2 h to obtain TiO_2 nanoparticles with a diameter of ~600 nm (TiO_2-600 nanoparticles).

Fabrication of Superhydrophobic Foams. Superhydrophobic foams were fabricated through the procedure described in reference 37. Briefly, 100 mg of TiO_2 nanoparticles (the mass ratio of TiO_2-600 to TiO_2-30 was 4:1) were dispersed in 10 mL of deionized water by sonication for 1 h. Later, 40 mg of dopamine, 10 μL of *n*-dodecanethiol (dissolved in 10 mL ethanol), and three pieces of copper foams (0.8 × 0.8 × 0.2 cm) were added to the above dispersion under stirring. The pH of the resulting mixture was adjusted to 8 by NaOH. After stirring for 9–12 h, the foams were successively washed with deionized water and ethanol.

Measurements of the Supporting Force and the Limit Depth of the As-Prepared Foams. A piece of superhydrophobic copper foam was horizontally fixed to the holder on a high-sensitivity microelectromechanical balance (DCAT 21, DataPhysics), and 50 mL of water was placed in a glass container beneath the holder. The water moved upward at a rate of 200 $\mu m\ s^{-1}$ until it reached the preset value of 8 mm, and then it moved downward to the original position at the same speed. The initial force and immersion depth of the foam in air were all set to zero. During the measurement, the foam first contacted with the water surface, then it penetrated the surface and immersed in the water. A CCD camera was also used to record the entire process. The supporting force and the limit depth of the foam at the water/air interface were collected by the balance.

To measure the supporting force and the limit depth of a superhydrophilic foam at the water/$CHCl_3$ interface, we conducted similar measurements by using a mixture of $CHCl_3$ and water placed in a glass container right below the holder. Before the measurements, the foam was immersed in the water, and its initial supporting force and immersion depth were all set to zero.

Characterizations. A scanning electron microscope (SEM, FEI Quanta 200) was employed to observe the morphology of the as-prepared foams. X-ray diffraction (XRD) patterns were recorded by a Shimadzu XRD-6000 diffractometer. X-ray photoelectron spectroscopy (XPS) data were collected with a PHI-5700ESCA electron spectrometer. Contact angles of the foams were measured by an OCA 20 (DataPhysics).

RESULTS AND DISCUSSION

The supporting legs of the strider were fabricated by directly anchoring TiO_2 nanoparticles and *n*-dodecanethoil onto the surface of copper foams through a mussel-inspired process (Scheme 1).[37] In a typical experiment, copper foams were immersed in an aqueous dopamine solution containing TiO_2 nanoparticles and *n*-dodecanethiol. After stirring for 9–12 h, the foams were successively washed with water and ethanol. At first, the chemical composition and microstructure of the resulting foams were investigated by XRD, SEM, and XPS measurements. Figure 1a is an XRD pattern of the resulting foams, which shows the feature peaks of TiO_2 phase, copper and nickel. The SEM images and energy dispersed spectroscopy (EDS) maps in Figure 1b–f display that the skeleton of the foams is homogeneously coated with TiO_2 nanoparticles of hundreds nanometers in diameter, and these nanoparticles form a porous appearance. XPS results also reveal that the surface of TiO_2 nanoparticles are grafted by thiolate moiety with alkyl tails (Supporting Information, Figure S1). All these results suggest that TiO_2 nanoparticles, together with *n*-dodecanethiol molecules, are directly immobilized onto the skeleton of copper foams through a single solution-immersion process. The immobilization process is associated with covalent and noncovalent interactions between copper, dopamine, thiol, and TiO_2.[37] Consequently, no TiO_2 nanoparticles were anchored on the surface of a copper foam in the absent of dopamine (Supporting Information, Figure S2). Then, the wetting properties of the resulting foams were measured by a contact angle instrument (OCA-20). As expected, these foams exhibited superhydrophobicity under ambient conditions because a water droplet (3 μL) could easily roll off their surfaces, showing a typical "lotus effect". The water contact angle (CA) and sliding angle (SA) of the foams were 152.7 ± 2.1° and 2.9 ± 1.7°, respectively.

The water contact angles of the resulting foams are strongly dependent on the size distribution of the immobilized TiO_2 nanoparticles. Here, we used TiO_2 nanoparticles of ~600 nm (TiO_2-600) and ~30 nm (TiO_2-30) to control the size distribution of the immobilized nanoparticles (Supporting Information, Figure S3). By simply tuning the mass ratio of TiO_2-600 to TiO_2-30 nanoparticles, we obtained copper foams

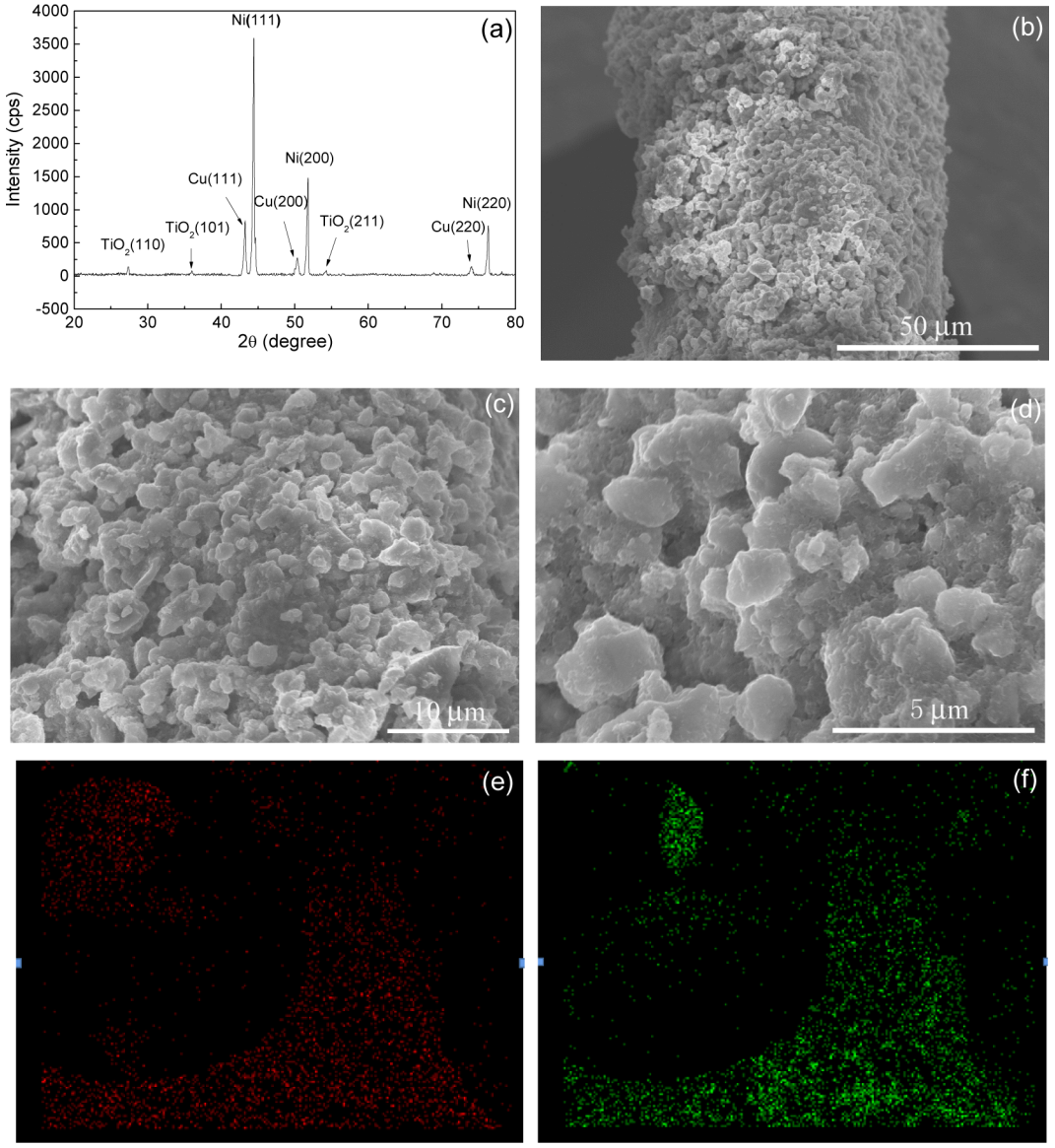

Figure 1. (a) XRD pattern, (b–d) SEM images, and (e) O and (f) Ti EDS maps of a superhydrophobic copper foam. The foam was fabricated from TiO_2-600 and TiO_2-30 with a mass ratio of 4:1.

with different contact angles. For instance, a foam exhibited a CA of 145.2 ± 1.8° or 150 ± 1.9° when only TiO_2-30 or TiO_2-600 nanoparticles were immobilized on its surface, respectively (Figure 2e–f). In contrast, a foam showed superhydrophobicity (CA = 152.7 ± 2.1°, SA = 2.9 ± 1.7°) when the TiO_2-600/TiO_2-30 mass ratio was 4:1. The reason for the difference is that the surface roughness of the foams is governed by the size of the immobilized TiO_2 nanoparticles (Figure 2a–d), which in turn affects their hydrophobicity. In addition, the superhydrophobic foams exhibited good durability to ultrasonication and chemical solvents like $CHCl_3$ (Supporting Information, Figures S4 and S5).

Interestingly, a superhydrophobic foam switched its wettability to superhydrophilicity (with a water contact angle of 0°) after ultraviolet (UV, 254 nm, 3W) illumination for 2 h. Indeed, a water drop (3 μL) was completely absorbed by the foam in a few seconds after the illumination (Figure 3a). However, a droplet of chloroform ($CHCl_3$, 3 μL) kept quasi-spherical shape (CA = 160 ± 1.8°) when it was placed on the foam immersed in water (Figure 3b). Additionally, the oil droplet could easily roll off the surface of the foam (SA = 0.6 ± 0.3°), indicating underwater superoleophobicity and low adhesion of the foam to $CHCl_3$. It is notable that the mass ratio of TiO_2-600 to TiO_2-30 has little impact on the underwater superoleophobicity (Figure 3c,d). Interestingly, the UV-irradiated foam regained superhydrophobicity after drying at 120 °C. The superhydrophobicity/underwater superoleophobicity transition could be repeated for seven cycles in this case, indicating good reversibility of the surface wettability (Supporting Information, Figure S6). To further investigate the repellent properties of the foam to $CHCl_3$ or water, we tested the adhesion force between them by a high sensitivity microelectromechanical balance (DCAT-21, Dataphysics). An adhesion force of ~36 μN is measured when the foam comes into contact with a water droplet in air (Figure 3e). In contrast, the foam shows a very low adhesion force (<8 μN) to a $CHCl_3$ droplet in water, as no force drop is observed in Figure 3f, suggesting that the foam exhibits much better antiadhesion performance to oils than to water. The above results demonstrate UV switchable super-

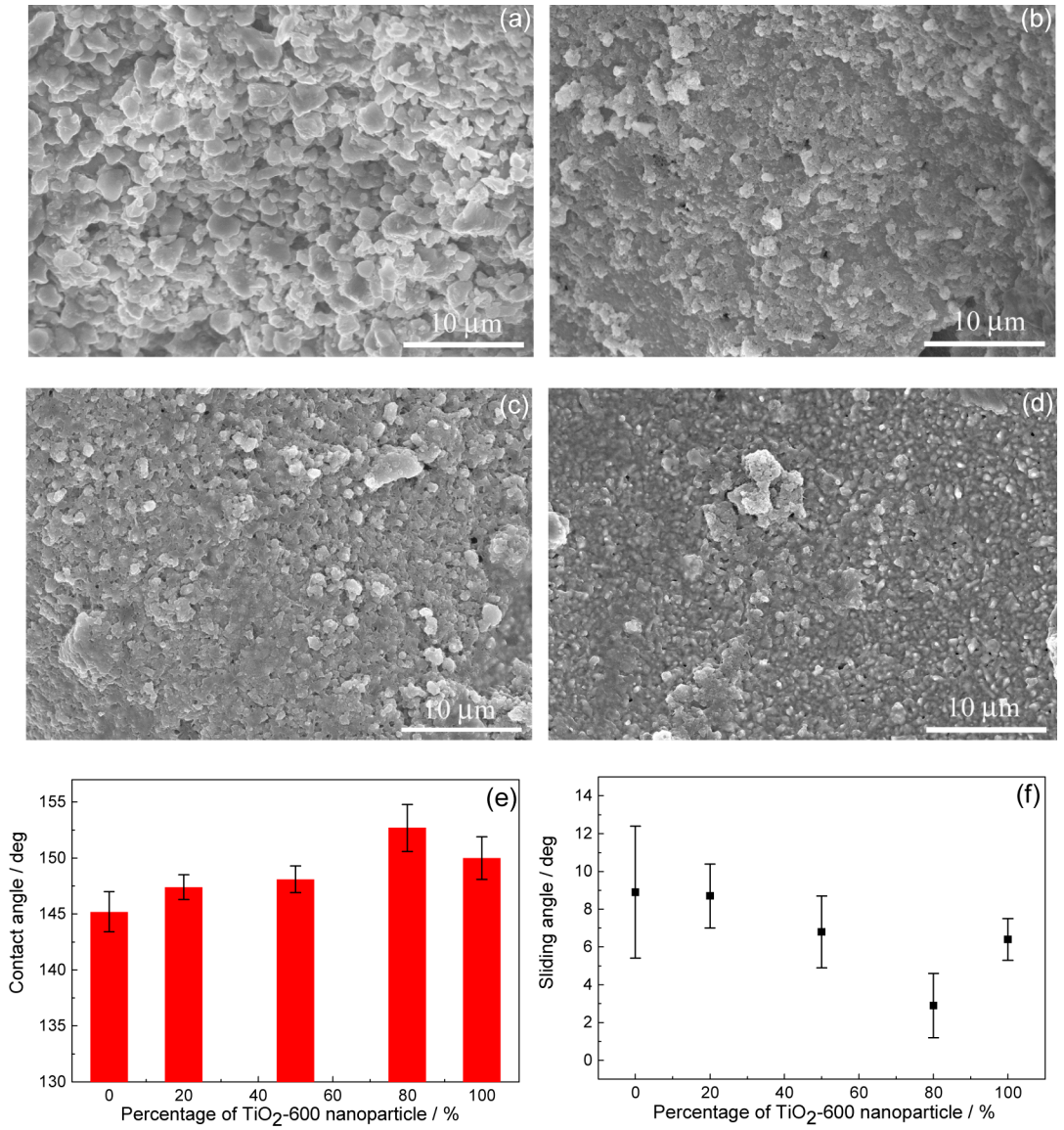

Figure 2. (a–d) Influence of mass ratio of TiO_2-600 to TiO_2-30 nanoparticles on the surface morphology: (a) TiO_2-600/TiO_2-30 = 1:0; (b) TiO_2-600/TiO_2-30 = 1:1; (c) TiO_2-600/TiO_2-30 = 1:4; and (d) TiO_2-600/TiO_2-30 = 0:1. (e) Water contact angle and (f) sliding angle of the as-prepared copper foams.

hydrophobicity/underwater superoleophobicity of the foam, as well as its low adhesion to water and $CHCl_3$.

The switchable wettability is ascribed to the photosensitivity of the immobilized TiO_2 nanoparticles, as the morphology of the foam did not change before and after the UV irradiation. Before UV irradiation, the surface of the TiO_2 nanoparticles is grafted with thiolate moiety with alkyl tails. According to Wenzel-Cassie equation, porous appearance of the TiO_2 nanoparticles together with low-energy alkyl tails confers the foam superhydrophobicity. After UV irradiation, the TiO_2 nanoparticles generate holes that readily react with lattice oxygen, which results in surface oxygen vacancies. The resulting vacancies coordinate to water molecules and thus greatly increasing hydrophilicity of the nanoparticles. High hydrophilicity allows water to fill in the interstices between the TiO_2 nanoparticles and replace the trapped air. The filled water minimizes the $CHCl_3$/TiO_2 contact area and thus leads to underwater superoleophobicity. However, the coordination with water makes the surface of the TiO_2 nanoparticles in the metastable state, which allows the coordinated water to be replaced by atmospheric oxygen.[38,21] As a result, the TiO_2 nanoparticles return to hydrophobicity, and the foam recovers its superhydrophobicity after drying at 120 °C.

Then, we fabricated an artificial strider by using the resultant foams as supporting legs and investigated its floating behavior on water and $CHCl_3$, respectively. The strider not only stood freely on a water surface but also could move around the surface without sinking (Figure 4a,b). The floating capability of the strider is related to high repellence of the legs to water because four dimples are observed on the water surface. These dimples display much larger displacement volumes than the corresponding legs (Figure 4a), producing sufficient buoyancy forces to support the strider. After UV irradiation for 2 h, the strider slowly dove into water as the legs changed their wettability to superhydrophilicity. Interestingly, the strider stopped diving but rather stayed stably on the oil (Figure 4c and movie, Supporting Information). Like on the water surface, the legs also formed four dimples on the oil due to underwater

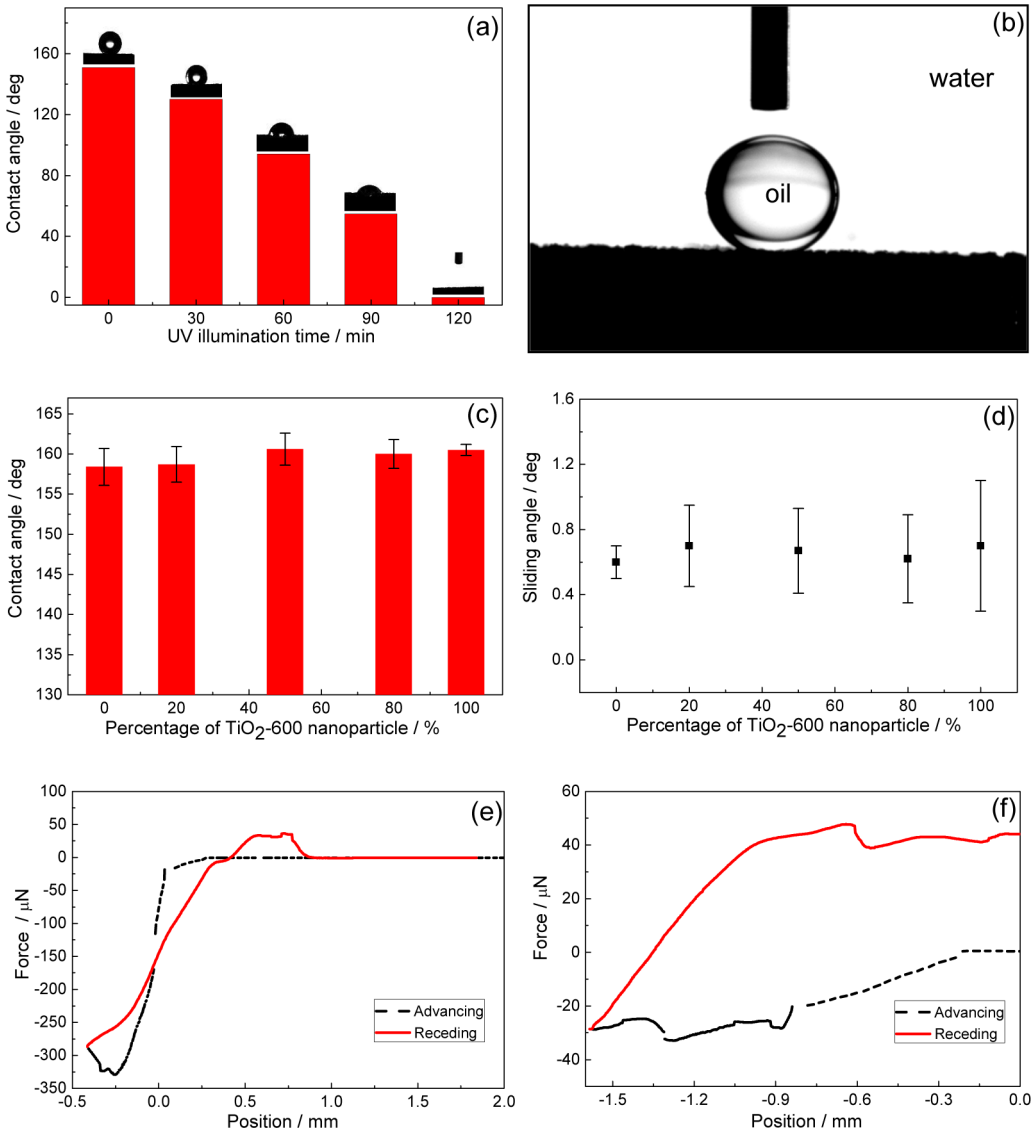

Figure 3. (a) Water contact angle of the foam during UV irradiation. (b) Contact angle of a $CHCl_3$ droplet on the foam after UV irradiation for 2 h. Effect of TiO_2-600/TiO_2-30 mass ratio on (c) contact angle and (d) sliding angle of the foam for $CHCl_3$ droplets. Adhesive force of the foam for (e) a water droplet and (f) a $CHCl_3$ droplet. The foam was fabricated from TiO_2-600 and TiO_2-30 with a mass ratio of 4:1.

Figure 4. Optical images for the artificial strider (a and b) floating on the water surface and (c) at the water/$CHCl_3$ interface. The $CHCl_3$ layer was dyed red by Rhodamine B for clear observation.

superoleophobicity. The displacement volumes of the dimples are also larger than those of the legs, providing sufficient supporting forces for the strider. These results suggest that an artificial strider can work on both water and oils by using the supporting legs with switchable superhydrophobicity/underwater superoleophobicity.

The force exerted on a supporting leg was systematically measured by a highly sensitive microelectromechanical balance (DCAT 21, Dataphysics), as shown in Figure S7 (Supporting Information). A CCD camera was also employed to record the cross-sectional view of the leg just before it penetrated the water/air or water/$CHCl_3$ interface. At first, the leg was horizontally fixed in the balance. Then, the water surface was moved upward at a speed of 200 μm s^{-1} until the leg reached a depth of 8.0 mm. The leg contacted with the water surface and then formed a dimple (Figure 5a, inset). The dimple became deeper until the leg penetrated the water surface and immersed in water. In this process, the measured force increased continuously and then reduced to 905 μN dramatically. A maximal supporting force of 4066 μN was measured at the depth of 4.17 mm (Figure 5a), much larger than the buoyant force produced by the leg itself (i.e., 905 μN). Therefore, superhydrophobicity offers a supporting force 4.5 times greater than the buoyant force. Then, we measured the supporting force at the water/$CHCl_3$ interface through the same method. The limit depth and the maximum supporting force at the interface are 4.65 mm and 2126 μN (Figure 5b), respectively. The latter is about 2.6 times the buoyancy force in $CHCl_3$ (810 μN). Figure 5c,d shows the dependence of the maximum force

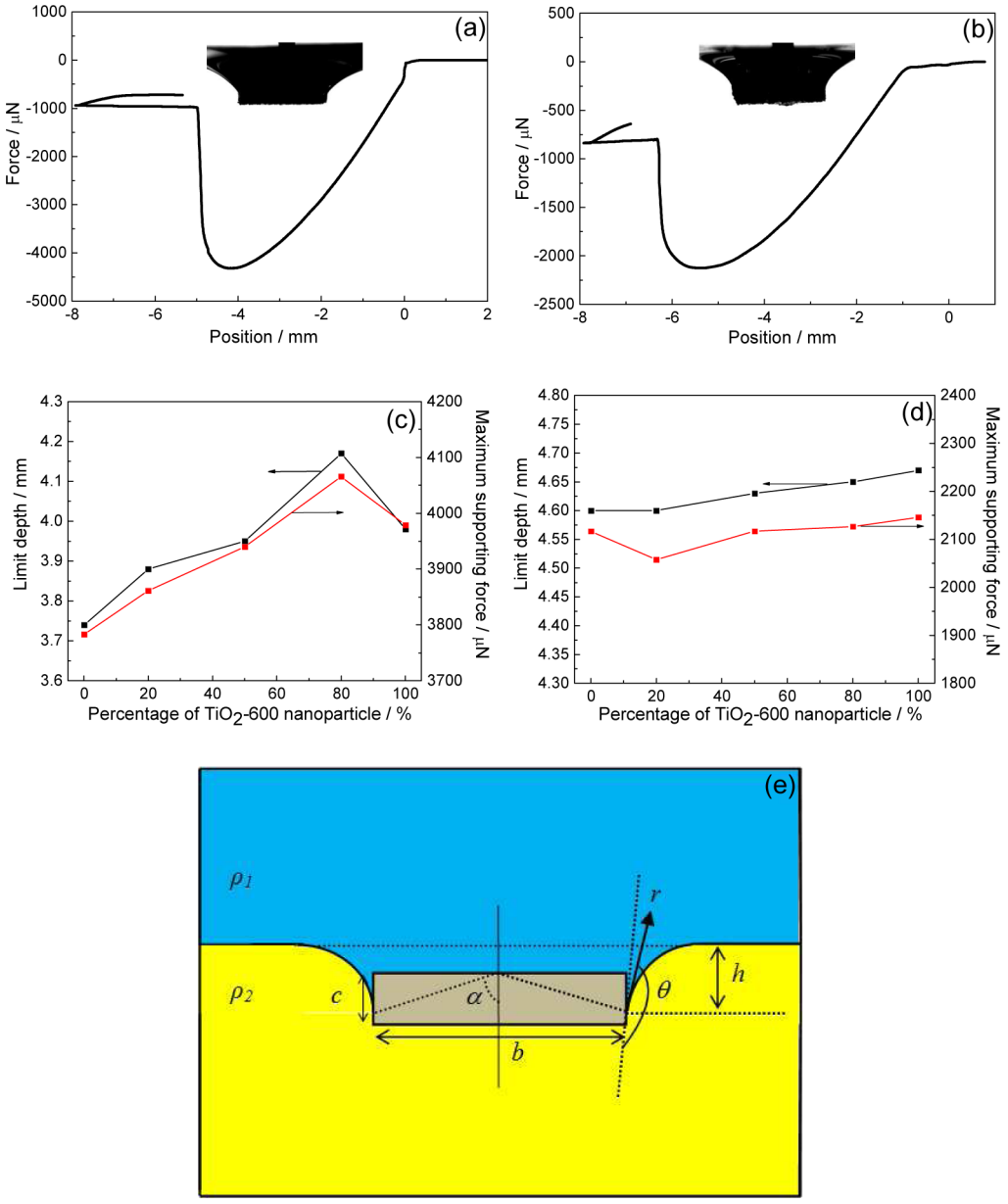

Figure 5. Force received by a supporting leg when it passes through the (a) water/air or (b) water/$CHCl_3$ interfaces. (Insets) Photographs recorded the limit depths of the leg at the corresponding interfaces. Effect of TiO_2-600/TiO_2-30 mass ratio on the limit depth and the maximum supporting force of the leg at the (c) water/air and (d) water/$CHCl_3$ interfaces. (e) Illustration of the cross-sectional view of the leg passing through the water/air or water/$CHCl_3$ interfaces; γ is the interfacial tension, α is the angle between the vertical line and the line starting from the top center of the leg to the point where the interface is separated by the leg, and θ is the contact angle of the leg for water or $CHCl_3$.

and the limit depth on the mass ratio of TiO_2-600 and TiO_2-30, suggesting that they are generally positively related.

Figure 5e show the force analysis of the leg at the water/air or water/$CHCl_3$ interface. Because the leg produces similar dimples at both interfaces, the received supporting force (F_s) can be analyzed through the model described previously.[3,8−10,39] For a rigid leg has the size of $a \times b \times c$, F_s mainly includes buoyancy force (F_b) and curvature force (F_c; eq 1).

$$F_s = F_c + F_b \tag{1}$$

$$F_c = -2\gamma \cos(a + \theta) \tag{2}$$

$$F_b = \rho_1 gabc + (\rho_2 - \rho_1)ghab + (\rho_2 - \rho_1)gab(h + c - \frac{1}{2}b \cot \alpha) \tag{3}$$

where ρ_1 is the density of air (for water/air interface) or water (for water/$CHCl_3$ interface), ρ_2 is the density of water (for water/air interface) or oil (for water/$CHCl_3$ interface), γ is the interfacial tension of water/air or water/$CHCl_3$ interface, θ is the contact angle of the leg for water or $CHCl_3$, and h and α are symbols used to the analysis with no physical meanings.

As shown in eq 2, curvature force F_c is strongly related to the contact angle θ of the leg for water or $CHCl_3$. An increase in θ will lead to a larger F_c. Considering that F_c will determine the limit depth of the leg at the water/air or water/$CHCl_3$ interface, θ also exerts an important impact on F_b. Equation 3 shows that

F_b is not only dependent on the size (a, b, c) of the leg, but it is also related to h and α that are governed by the θ of the leg at the water/air or water/$CHCl_3$ interface. For example, both immersion depth and supporting force become larger as θ increases (Figure 5c,d). In this case, the leg reaches its maximum in immersion depth and supporting force when θ for water and $CHCl_3$ is 152.7 ± 2.1° and 160.7 ± 0.7°, respectively. Nevertheless, once the leg is completely wetted by $CHCl_3$ or water (i.e., $\theta \approx 0$), α is closed to 90°, and the limit depth of the leg becomes too little to be taken into account. As a result, both F_c and F_b are negligible and thus lead to a small F_s. Because θ is governed by both surface morphology and wettability of the leg, constructing micro/nanohierarchical structures is very important for a large F_s at the water/air or water/$CHCl_3$ interface. Such hierarchical structures induce high repellency for water or oils, which prevents the leg from being penetrated by the liquids and increases its limit depth at the interfaces. More importantly, hydrophobicity/hydrophilicity switch enables the leg to achieve a large F_s at different interfaces.

CONCLUSIONS

In summary, using copper foams with UV switchable wettability as supporting legs, a smart strider could float at both water/air and water/oil interfaces for the first time. By controlling superhydrophobicity or superhydrophilicity of the legs, we developed legs that exhibited superior repellence to water or oils and produced a supporting force about 2.6−4.5 times the maximal buoyant force they received. The large supporting force is associated with micro/nanohierarchical structures and photosensitivity of the immobilized TiO_2 nanoparticles. Considering simplicity and versatility of the mussel-inspired process, the concept is extendable to fabricate intelligently interfacial materials on other substrates (e.g., nickel foam and polyurethane sponge) using various photosensitive nanoparticles like ZnO[40,41] and V_2O_5.[42] The present findings also offer an alternative and facile strategy for designing smart miniaturized devices for water environmental protection and oil spillage cleanup, as well as for fabricating drag-reducing materials, and so on.

ASSOCIATED CONTENT

Supporting Information

XPS results and EDS plot of the superhydrophobic foam; SEM images of the copper foam prepared without dopamine; TEM images of TiO_2-30 and TiO_2-600 nanoparticles; effect of ultrasonication and immersion in $CHCl_3$ on the morphology and water contact angle; reversible superhydrophobicity/underwater superoleophobicity switch of the foams; and schematic diagram for the measurement of supporting force at the water/air or water/$CHCl_3$ interface. This material is available free of charge via the Internet at http://pubs.acs.org.

AUTHOR INFORMATION

Corresponding Author

*E-mail: panqm@hit.edu.cn.

Notes

The authors declare no competing financial interest.

ACKNOWLEDGMENTS

This work was financially supported by a self-planned task of the State Key Laboratory of Robotics and Systems of the Harbin Institute of Technology (Grant SKLRS200901C) and the National Natural Science Foundation of China (51473041).

REFERENCES

(1) Dickinson, M. Animal Locomotion: How to Walk on Water. *Nature* **2003**, *424*, 621−622.
(2) Gao, X. F.; Jiang, L. Biophysics: Water-Repellent Legs of Water Striders. *Nature* **2004**, *432*, 36.
(3) Shi, F.; Niu, J.; Liu, J. L.; Liu, F.; Wang, Z. Q.; Feng, X. Q.; Zhang, X. Towards Understanding Why a Superhydrophobic Coating Is Needed by Water Striders. *Adv. Mater.* **2007**, *19*, 2257−2261.
(4) Shi, F.; Wang, Z. Q.; Zhang, X. Combining a Layer-by-Layer Assembling Technique with Electrochemical Deposition of Gold Aggregates to Mimic the Legs of Water Striders. *Adv. Mater.* **2005**, *17*, 1005−1009.
(5) Jiang, L.; Yao, X.; Li, H. X.; Fu, Y. Y.; Chen, L.; Meng, Q.; Hu, W. P. Water Strider Legs with a Self-Assembled Coating of Single-Crystalline Nanowires of an Organic Semiconductor. *Adv. Mater.* **2010**, *22*, 376−379.
(6) Wu, X. F.; Shi, G. Q. Production and Characterization of Stable Superhydrophobic Surfaces Based on Copper Hydroxide Nanoneedles Mimicking the Legs of Water Striders. *J. Phys. Chem. B* **2006**, *110*, 11247−11252.
(7) Pan, Q. M.; Liu, J.; Zhu, Q. A Water Strider-Like Model with Large and Stable Loading Capacity Fabricated from Superhydrophobic Copper Foils. *ACS Appl. Mater. Interfaces* **2010**, *2*, 2026−2030.
(8) Zhao, J.; Zhang, X. B.; Chen, N.; Pan, Q. M. Why Superhydrophobicity Is Crucial for a Water-Jumping Microrobot? Experimental and Theoretical Investigations. *ACS Appl. Mater. Interfaces* **2012**, *4*, 3706−3711.
(9) Zhang, X. B.; Zhao, J.; Zhu, Q.; Chen, N.; Zhang, M. W.; Pan, Q. M. Bioinspired Aquatic Microrobot Capable of Walking on Water Surface Like a Water Strider. *ACS Appl. Mater. Interfaces* **2011**, *3*, 2630−2636.
(10) Liu, X. L.; Gao, J.; Xue, Z. X.; Chen, L.; Lin, L.; Jiang, L.; Wang, S. T. Bioinspired Oil Strider Floating at the Oil/Water Interface Supported by Huge Superoleophobic Force. *ACS Nano* **2012**, *6*, 5614−5620.
(11) Liu, M. J.; Wang, S. T.; Wei, Z. X.; Song, Y. L.; Jiang, L. Bioinspired Design of a Superoleophobic and Low Adhesive Water/Solid Interface. *Adv. Mater.* **2009**, *21*, 665−669.
(12) Jin, H.; Kettunen, M.; Laiho, A.; Pynnonen, H.; Paltakari, J.; Marmur, A.; Ikkala, O.; Ras, R. H. A. Superhydrophobic and Superoleophobic Nanocellulose Aerogel Membranes as Bioinspired Cargo Carriers on Water and Oil. *Langmuir* **2011**, *27*, 1930−1934.
(13) Zhang, J. H.; Deng, X.; Butt, H. J.; Vollmer, D. Floating on Oil. *Langmuir* **2014**, *30*, 10637−10642.
(14) Chu, Z. L.; Seeger, S. Superamphiphobic Surfaces. *Chem. Soc. Rev.* **2014**, *43*, 2784−2798.
(15) Deng, X.; Mammen, L.; Butt, H.-J.; Vollmer, D. Candle Soot as a Template for a Transparent Robust Superamphiphobic Coating. *Science* **2012**, *335*, 67−70.
(16) Wang, H. X.; Xue, Y. H.; Ding, J.; Feng, L. F.; Wang, X. G.; Lin, T. Durable, Self-Healing Superhydrophobic and Superoleophobic Surfaces from Fluorinated-Decyl Polyhedral Oligomeric Silsesquioxane and Hydrolyzed Fluorinated Alkyl Silane. *Angew. Chem., Int. Ed.* **2011**, *50*, 11433−11436.
(17) Zhou, H.; Wang, H. X.; Niu, H. T.; Gestos, A.; Lin, T. Robust, Self-Healing Superamphiphobic Fabrics Prepared by Two-Step Coating of Fluoro-Containing Polymer, Fluoroalkyl Silane, and Modified Silica Nanoparticles. *Adv. Funct. Mater.* **2013**, *23*, 1664−1670.
(18) Pan, S. J.; Kota, A. K.; Mabry, J. M.; Tuteja, A. Superomniphobic Surfaces for Effective Chemical Shielding. *J. Am. Chem. Soc.* **2013**, *135*, 578−581.
(19) Feng, X. J.; Jiang, L. Design and Creation of Superwetting/Antiwetting Surfaces. *Adv. Mater.* **2006**, *18*, 3063−3078.
(20) Xia, F.; Jiang, L. Bio-Inspired, Smart, Multiscale Interfacial Materials. *Adv. Mater.* **2008**, *20*, 2842−2858.

(21) Feng, X. J.; Zhai, J.; Jiang, L. The Fabrication and Switchable Superhydrophobicity of TiO_2 Nanorod Films. *Angew. Chem., Int. Ed.* **2005**, *44*, 5115−5118.
(22) Malm, J.; Sahramo, E.; Karppinen, M.; Ras, R. H. A. Photo-Controlled Wettability Switching by Conformal Coating of Nanoscale Topographies with Ultrathin Oxide Films. *Chem. Mater.* **2010**, *22*, 3349−3352.
(23) Lim, H. S.; Kwak, D.; Lee, D. Y.; Lee, S. G.; Cho, K. UV-Driven Reversible Switching of a Roselike Vanadium Oxide Film between Superhydrophobicity and Superhydrophilicity. *J. Am. Chem. Soc.* **2007**, *129*, 4128−4129.
(24) Zahner, D.; Abagat, J.; Svec, F.; Fréchet, J. M. J.; Levkin, P. A. A Facile Approach to Superhydrophilic−Superhydrophobic Patterns in Porous Polymer Films. *Adv. Mater.* **2011**, *23*, 3030−3034.
(25) Papadopoulou, E. L.; Barberoglou, M.; Zorba, V.; Manousaki, A.; Pagkozidis, A.; Stratakis, E.; Fotakis, C. Reversible Photoinduced Wettability Transition of Hierarchical ZnO Structures. *J. Phys. Chem. C* **2009**, *113*, 2891−2895.
(26) Li, C.; Zhang, Y. Y.; Ju, J.; Cheng, F. T.; Liu, M. J.; Jiang, L.; Yu, Y. L. In Situ Fully Light-Driven Switching of Superhydrophobic Adhesion. *Adv. Funct. Mater.* **2012**, *22*, 760−763.
(27) Rafiee, J.; Rafiee, M. A.; Yu, Z. Z.; Koratkar, N. Superhydrophobic to Superhydrophilic Wetting Control in Graphene Films. *Adv. Mater.* **2010**, *22*, 2151−2154.
(28) Xia, F.; Feng, L.; Wang, S. T.; Sun, T. L.; Song, W. L.; Jiang, W. H.; Jiang, L. Dual-Responsive Surfaces That Switch between Superhydrophilicity and Superhydrophobicity. *Adv. Mater.* **2006**, *18*, 432−436.
(29) Xia, F.; Ge, H.; Hou, Y.; Sun, T. L.; Chen, L.; Zhang, G. Z.; Jiang, L. Multiresponsive Surfaces Change Between Superhydrophilicity and Superhydrophobicity. *Adv. Mater.* **2007**, *19*, 2520−2524.
(30) Yu, X.; Wang, Z. Q.; Jiang, Y. G.; Shi, F.; Zhang, X. Reversible pH-responsive Surface: From Superhydrophobicity to Superhydrophilicity. *Adv. Mater.* **2005**, *17*, 1289−1293.
(31) Wang, S. T.; Liu, H. J.; Liu, D. S.; Ma, X. Y.; Fang, X. H.; Jiang, L. Enthalpy-Driven Three-State Switching of a Superhydrophilic/Superhydrophobic Surface. *Angew. Chem., Int. Ed.* **2007**, *46*, 3915−3917.
(32) Jiang, Y. G.; Wan, P. B.; Smet, M.; Wang, Z. Q.; Zhang, X. Self-Assembled Monolayers of a Malachite Green Derivative: Surfaces with pH- and UV-Responsive Wetting Properties. *Adv. Mater.* **2008**, *20*, 1972−1977.
(33) Xu, L. B.; Chen, W.; Mulchandani, A.; Yan, Y. S. Reversible Conversion of Conducting Polymer Films from Superhydrophobic to Superhydrophilic. *Angew. Chem., Int. Ed.* **2005**, *44*, 6009−6012.
(34) Kakade, B.; Mehta, R.; Durge, A.; Kulkarni, S.; Pillai, V. Electric Field Induced, Superhydrophobic to Superhydrophilic Switching in Multiwalled Carbon Nanotube Papers. *Nano Lett.* **2008**, *8*, 2693−2696.
(35) Yang, J.; Zhang, Z. Z.; Men, X. H.; Xu, X. H.; Zhu, X. T.; Zhou, X. Y. Counterion Exchange to Achieve Reversibly Switchable Hydrophobicity and Oleophobicity on Fabrics. *Langmuir* **2011**, *27*, 7357−7360.
(36) Lim, H. S.; Lee, S. G.; Lee, D. H.; Lee, D. Y.; Lee, S.; Cho, K. Superhydrophobic to Superhydrophilic Wetting Transition with Programmable Ion-Pairing Interaction. *Adv. Mater.* **2008**, *20*, 4438−4441.
(37) Zhu, Q.; Pan, Q. M. Mussel-Inspired Direct Immobilization of Nanoparticles and Application for Oil-Water Separation. *ACS Nano* **2014**, *8*, 1402−1409.
(38) Wang, R.; Sakai, N.; Fujishima, A.; Watanabe, T.; Hashimoto, K. Studies of Surface Wettability Conversion on TiO_2 Single-Crystal Surfaces. *J. Phys. Chem. B* **1999**, *103*, 2188−2194.
(39) Hu, D. L.; Chan, B.; Bush, J. W. M. The Hydrodynamics of Water Strider Locomotion. *Nature* **2003**, *424*, 663−666.
(40) Feng, X. J.; Feng, L.; Jin, M. H.; Zhai, J.; Jiang, L.; Zhu, D. B. Reversible Superhydrophobicity to Superhydrophilicity Transition of Aligned ZnO Nanorod Films. *J. Am. Chem. Soc.* **2004**, *126*, 62−63.
(41) Sun, Z. Q.; Liao, T.; Liu, K. S.; Jiang, L.; Kim, J. H.; Dou, S. X. Robust Superhydrophobicity of Hierarchical ZnO Hollow Microspheres Fabricated by Two-Step Self-Assembly. *Nano Research* **2013**, *6*, 726−735.
(42) Lim, H. S.; Kwak, D.; Lee, D. Y.; Lee, S. G.; Cho, K. UV-Driven Reversible Switching of a Roselike Vanadium Oxide Film between Superhydrophobicity and Superhydrophilicity. *J. Am. Chem. Soc.* **2007**, *129*, 4128−4129.